nature chemistry

Article

https://doi.org/10.1038/s41557-024-01608-8

A metalloenzyme platform for catalytic asymmetric radical dearomatization

Received: 2 August 2023

Accepted: 17 July 2024

Published online: 28 August 2024

Check for updates

Wenzhen Fu[1], Yue Fu[2,4], Yunlong Zhao[1,4], Huanan Wang[1], Peng Liu[2] ✉ & Yang Yang[1,3] ✉

Catalytic asymmetric dearomatization represents a powerful means to convert flat aromatic compounds into stereochemically well-defined three-dimensional molecular scaffolds. Using new-to-nature metalloredox biocatalysis, we describe an enzymatic strategy for catalytic asymmetric dearomatization via a challenging radical mechanism that has eluded small-molecule catalysts. Enabled by directed evolution, new-to-nature radical dearomatases $P450_{rad1}$–$P450_{rad5}$ facilitated asymmetric dearomatization of a broad spectrum of aromatic substrates, including indoles, pyrroles and phenols, allowing both enantioconvergent and enantiodivergent radical dearomatization reactions to be accomplished with excellent enzymatic control. Computational studies revealed the importance of additional hydrogen bonding interactions between the engineered metalloenzyme and the reactive intermediate in enhancing enzymatic activity and enantiocontrol. Furthermore, designer non-ionic surfactants were found to significantly accelerate this biotransformation, providing an alternative means to promote otherwise sluggish new-to-nature biotransformations. Together, this evolvable metalloenzyme platform opens up new avenues to advance challenging catalytic asymmetric dearomatization processes involving free radical intermediates.

Aromaticity represents a fundamental concept with broad implications spanning all disciplines of chemistry[1]. The disruption of aromaticity is thermodynamically unfavourable and therefore oftentimes challenging. Nevertheless, catalytic asymmetric dearomatization of flat aromatics can lead to the stereoselective construction of valuable three-dimensional molecular complexities, thus holding important potential to streamline the preparation of stereochemically complex bioactive agents[2]. Over the past two decades, pioneering research on transition metal catalysis and organocatalysis has afforded powerful methods for asymmetric dearomatization using two-electron mechanisms[3–6]. By contrast, despite notable recent progress based on stoichiometric chiral radical initiating reagents[7,8], catalytic asymmetric dearomatization via a free radical mechanism has remained a daunting task, mainly due to the challenges in exerting stereocontrol over highly reactive radical intermediates[9–11].

Due to the numerous potentially cooperative interactions between the enzyme scaffold and the reactive intermediate that can be readily exploited by directed evolution[12], biocatalysis has been recognized as a promising alternative to tackle challenging problems in asymmetric synthesis[13,14]. Previous elegant studies have established Rieske dioxygenases[15–17], flavin-dependent monooxygenases[18] and SAM/cobalamin-dependent systems for oestrogen methylation[19] as valuable stereoselective biocatalysts for the oxidative dearomatization of aromatic compounds (Fig. 1a). To further expand the repertoire of biocatalytic dearomatization, we sought to leverage enzymatic mechanisms[20–38] to address key challenges in asymmetric radical dearomatization under non-oxidative conditions.

Recently, we questioned whether we could advance a unifying enzymatic strategy for the asymmetric radical dearomatization of a wide

[1]Department of Chemistry and Biochemistry, University of California, Santa Barbara, CA, USA. [2]Department of Chemistry, University of Pittsburgh, Pittsburgh, PA, USA. [3]Biomolecular Science and Engineering (BMSE) Program, University of California, Santa Barbara, CA, USA. [4]These authors contributed equally: Yue Fu, Yunlong Zhao. ✉e-mail: pengliu@pitt.edu; yang@chem.ucsb.edu

https://doi.org/10.1038/s41557-024-01608-8

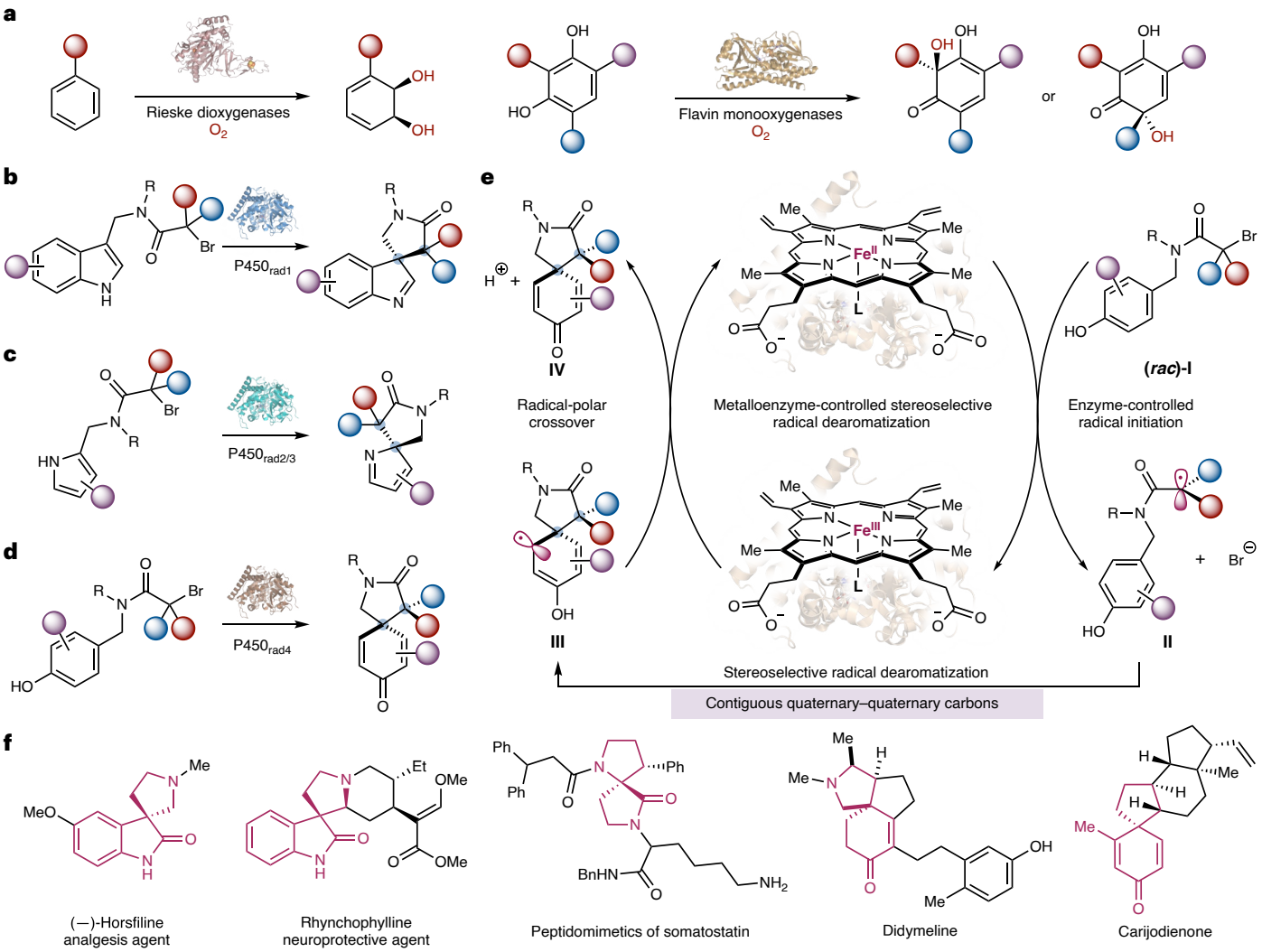

Fig. 1 | Catalytic asymmetric radical dearomatization using metalloredox biocatalysis. a, Biocatalytic dearomatization under oxidative conditions: natural enzymatic activities. **b**, New-to-nature biocatalytic asymmetric radical dearomatization of indoles. **c**, New-to-nature biocatalytic asymmetric radical dearomatization of pyrroles. **d**, New-to-nature biocatalytic asymmetric radical dearomatization of phenols. **e**, Proposed catalytic cycle with new-to-nature P450 radical dearomatases. **f**, Selected bioactive compounds with a chiral spirocyclic backbone. L, Fe-binding amino acid residue; in this work, L is serine. Red, blue and purple spheres are generic substituents of the molecule. The spirocyclic backbones are highlighted in magenta in **f**.

range of aromatic and heteroaromatic compounds using metalloredox biocatalysis (Fig. 1b–d). Inspired by related studies in synthetic organic chemistry[4], the overall catalytic cycle of this metalloenzyme-catalysed unnatural radical dearomatization is described in Fig. 1e. Similar to our recently reported radical cyclases[20,21,23], first, the ferrous haem protein catalyst reduces the α-bromocarbonyl substrate **I** via a halogen atom or electron transfer mechanism, providing a highly reactive radical species **II** along with the ferric haem enzyme. This nascent electrophilic radical **II** subsequently undergoes cyclization with the electron-rich arene or heteroarene, giving rise to a dearomatized radical intermediate **III**. Finally, oxidative radical-polar crossover of **III** and proton transfer furnishes the final dearomatized product **IV**. Meanwhile, this step also regenerates the ferrous protein catalyst and completes the catalytic cycle. If successfully implemented, this biocatalytic radical dearomatization would afford stereochemical dyads featuring contiguous quaternary–quaternary stereocentres[39,40], a challenging process for catalytic asymmetric dearomatization. Furthermore, the selective assembly of such vicinal quaternary–quaternary stereocentres has long been regarded as a demanding task in asymmetric catalysis[39,40], for which free radical chemistry has rarely been explored. Due to the outstanding tunability of cytochrome P450 enzymes[41–44], we posited that through directed evolution, we could engineer P450 radical dearomatases ($P450_{rad}$) to impose stereocontrol over the formation of either quaternary centre (Fig. 1e). Moreover, we envisioned that a panel of customized P450 radical dearomatases could be evolved, accommodating a wide range of electron-rich aromatic and heteroaromatic substrates, thereby providing an enzymatic platform for the asymmetric synthesis of spirocyclic compounds widely incorporated into bioactive natural products and medicinal agents (Fig. 1f)[45,46].

Results

Discovery and engineering of indole dearomatase $P450_{rad1}$

At the outset of this study, we focused our efforts on biocatalytic radical dearomatization of indoles, an essential class of nitrogen heterocycles with broad utility in pharmaceuticals, agrochemicals and functional materials (Fig. 2)[47]. Using α-bromoamide-appended indole **1a** as the model substrate, we evaluated a panel of previously engineered CYP102A1 (cytochrome $P450_{BM3}$) variants, including our recently engineered P450 radical cyclases[20,23]. This initial biocatalyst evaluation was performed using intact *Escherichia coli* cells harbouring the specific P450 variant in 96-well plates in a high-throughput format (Fig. 2a). The desired spirocyclic dearomatized product **2a**

https://doi.org/10.1038/s41557-024-01608-8

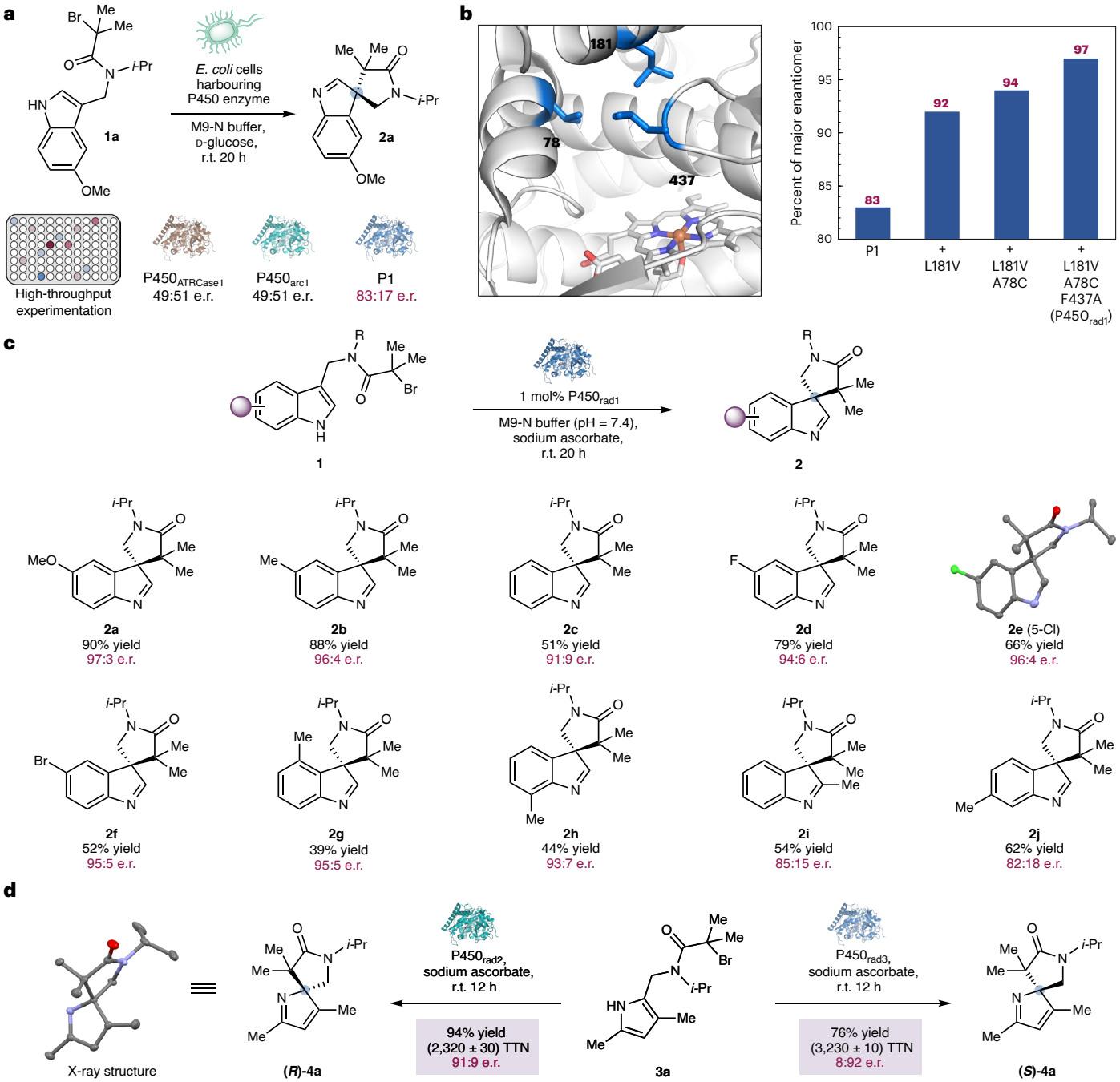

Fig. 2 | Discovery, directed evolution and substrate scope of $P450_{rad1}$, $P450_{rad2}$ and $P450_{rad3}$. a, Evaluation of P450 biocatalysts for enantioselective radical dearomatization of indole **1a**. **b**, Directed evolution of indole radical dearomatase $P450_{rad1}$. Active-site illustration (left) was made on the basis of the crystal structure of a closely related P450 variant (Protein Data Bank (PDB) no. 5UCW). **c**, Substrate scope of $P450_{rad1}$-catalysed enantioselective radical dearomatization of indoles. Conditions were as follows: **1** (5.0 mM), sodium ascorbate (5.0 mM) and $P450_{rad1}$ (1 mol%) as cell-free lysates in M9-N buffer (total volume, 400 µl). For **2g**, $P450_{rad1}$ A437F was used in lieu of $P450_{rad1}$. Enantioselectivities in **b** and **c** are from reactions with cell-free lysates (Supplementary Sections III and VI for details). 5-Cl indicates the chloride substituent in the C5 position of the indole ring. **d**, Biocatalytic enantiodivergent radical dearomatization of pyrroles using engineered pyrrole radical dearomatases $P450_{rad2}$ and $P450_{rad3}$. TTN, total turnover number. Conditions were as follows: **3a** (10.0 mM), sodium ascorbate (10.0 mM) and cell-free lysates with OD_{600} = 30 in M9-N buffer (total volume, 400 µl; Supplementary Tables 15 and 16 for details). r.t., room temperature. All the biocatalytic reactions were performed as technical triplicates. For X-ray crystal structures, thermal ellipsoids were set at 50% probability; hydrogen atoms are omitted for clarity. Supplementary Section VIII contains details.

featuring adjacent quaternary–quaternary carbons formed with many variants that we screened, mostly in a racemic form (Supplementary Table 1 for details). For example, our recently evolved P450 radical cyclases $P450_{ATRCase1}$ (ref. 20) and $P450_{arc1}$ (ref. 23) afforded **2a** in 35% and 38% yields, respectively, both in 49:51 enantiomeric ratio (e.r.). However, to our delight, P411-CIS I263G L437F V87L P248T ('P1'), a closely related variant of a previously engineered carbene transferase $P411\text{-}VAC_{trans}$ (ref. 48), furnished product **2a** in 34% yield and 53:47 e.r. (Supplementary Table 1). Additionally, biotransformations with cell-free lysates in the presence of supplemented sodium ascorbate were found to provide similar yields and enhanced enantioselectivity (83:17 e.r.).

https://doi.org/10.1038/s41557-024-01608-8

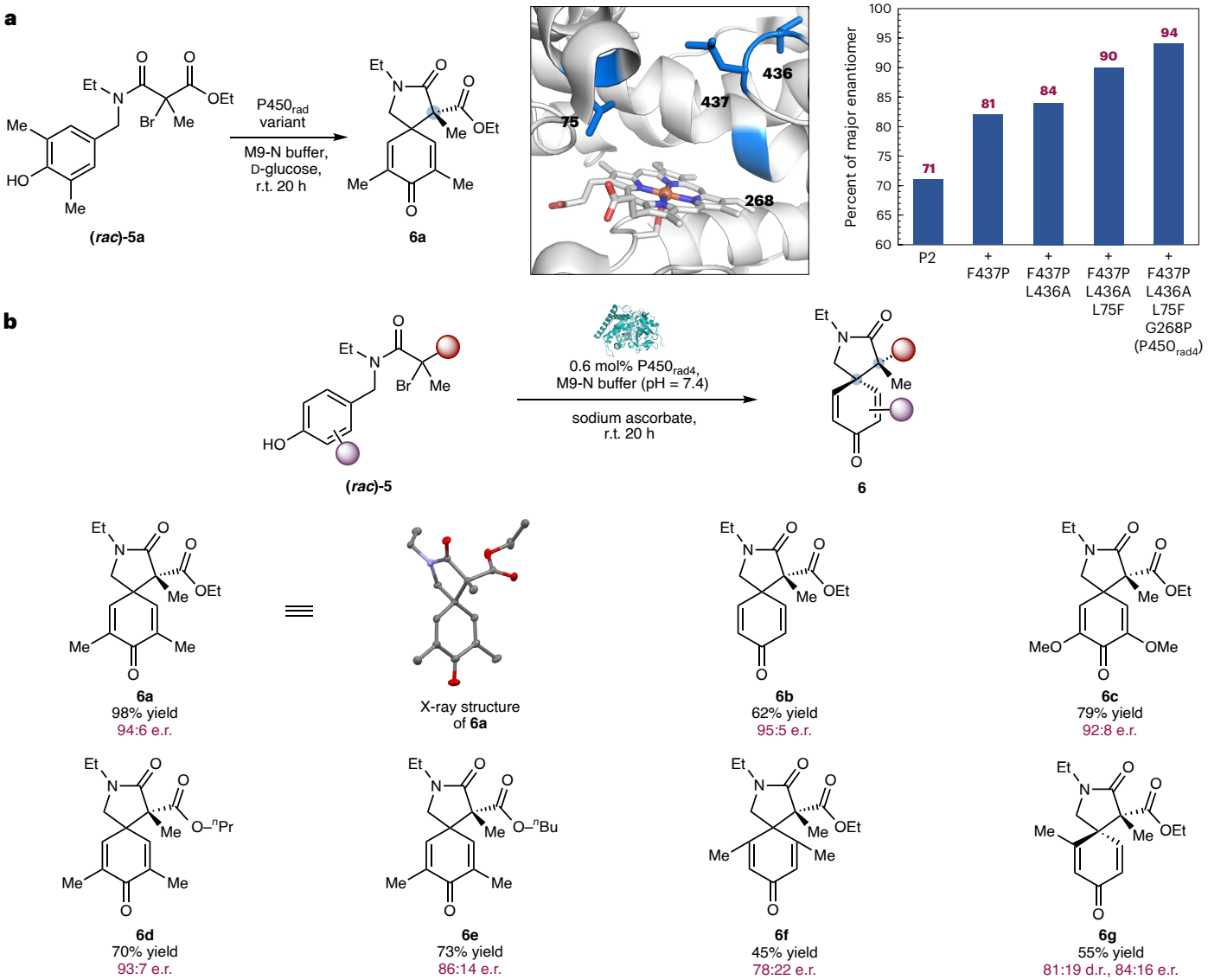

Fig. 3 | Directed evolution and substrate scope of P450$_{rad4}$. **a**, Directed evolution of enantioconvergent phenol radical dearomatase P450$_{rad4}$. Active site illustration (center) was made on the basis of the crystal structure of a closely related P450 variant (PDB no. 5UCW). **b**, Substrate scope of P450$_{rad4}$-catalysed enantioconvergent radical dearomatization of phenols. Conditions were as follows: **5** (5.0 mM), sodium ascorbate (5.0 mM) and P450$_{rad4}$ (0.6 mol%) as cell-free lysates in M9-N buffer (total volume, 400 µl). For **6f** and **6g**, P2 was used in lieu of P450$_{rad4}$. All the biocatalytic reactions were performed as technical triplicates. For X-ray crystal structures, thermal ellipsoids were set at 50% probability; hydrogen atoms are omitted for clarity. Supplementary Section VIII contains details.

With P1 as the parent, we embarked on a directed evolution campaign to improve the enantioselectivity and activity of this P450 radical dearomatase (Fig. 2b). Aided by molecular docking studies using AutoDock (Supplementary Section II for details), key active-site residues were targeted and subjected to iterative site-saturated mutagenesis and screening. In each round of directed evolution, four enzyme libraries were expressed and evaluated in 96-well plates. For each site-saturated mutagenesis library, 88 clones were selected and screened (Supplementary Table 5). Three beneficial mutations, including L181V, A78C and F437A, were identified, leading to P411-CIS A78C V87L L181V P248T I263G F437A, which we called P450$_{rad1}$ (rad = radical dearomatase). In the form of whole-cell biocatalyst, P450$_{rad1}$ provided a twofold improvement in activity and significantly higher enantioselectivity (82% yield and 91:9 e.r.; Supplementary Table 7 for further details). When the cell-free lysate of P450$_{rad1}$ was employed, **2a** was obtained in 90% yield and 97:3 e.r. (Fig. 2b,c; Supplementary Table 8 for further details). The 6-*endo-trig* radical cyclization to the indole C-2 position was not observed under these conditions.

With this newly evolved indole dearomatase P450$_{rad1}$, we next surveyed the substrate scope of biocatalytic enantioselective radical dearomatization of indoles to prepare spirocyclic products **2** bearing vicinal quaternary–quaternary carbons (Fig. 2c). Indoles possessing an electron-donating group at the 5 position, such as a methoxy (**2a**) and a methyl (**2b**), were excellent substrates, providing the desired dearomatized product in excellent yields and enantioselectivities. Electron-withdrawing functional groups such as a fluorine (**2d**), a chlorine (**2e**) and a bromine (**2f**) were also compatible. Furthermore, without further engineering, indoles bearing substituents at the 2, 4, 5, 6 and 7 positions could all be transformed smoothly by the dearomatases we engineered (**2g**–**2j**). Indoles with a 4-methyl (**2g**) and 7-methyl group were transformed with excellent enantioselectivity, although with slightly lower yields presumably due to the increased steric hindrance. For 4-methylindole (**2g**), an intermediate variant P1

A78C L181V ($P450_{rad1}$ A437F) provided slightly higher enantioselectivity (95:5 e.r.) than $P450_{rad1}$. Finally, the absolute stereochemistry of **2e** was ascertained by single-crystal X-ray diffraction analysis (Cambridge Crystallographic Data Centre (CCDC) no. 2245164).

Enantiodivergent pyrrole dearomatases $P450_{rad2}$ and $P450_{rad3}$

In addition, we found that this metalloenzyme platform could be readily applied to the radical dearomatization of other N-heterocycles, such as pyrroles (Fig. 2d). Notably, upon the evaluation of a small panel of P450 variants, a set of enantiodivergent dearomatases could be identified to afford either (***R***)-**4a** or (***S***)-**4a**. Specifically, P411-CIS L75A L181A furnished (***R***)-**4a** in 93% yield and 85:15 e.r., whereas the use of $P411_{Diane2}$ W263I G268A P327T V328A resulted in (***S***)-**4a** in 93% yield and 10:90 e.r. (Supplementary Tables 11 and 14). In only one round of engineering through site-saturation mutagenesis and screening, $P450_{rad2}$ and $P450_{rad3}$ could be developed to provide further enhanced enantioselectivity in the biocatalytic radical dearomatization of **3a** (Supplementary Tables 9–16 for details). With $P450_{rad2}$ (P411-CIS L75A L181A **A82V**), (***R***)-**4a** was produced in 94% yield, 91:9 e.r. and with a total turnover number of 2,320 ± 30 (Supplementary Table 15). On the other hand, (***S***)-**4a** formed in 76% yield, 8:92 e.r. and with a total turnover number of 3,230 ± 10 using $P450_{rad3}$ ($P411_{Diane2}$ W263I G268A P327T V328A **E267L;** Supplementary Table 16). Additionally, the absolute stereochemistry of (***R***)-**4a** was determined by X-ray diffraction analysis (CCDC no. 2245162). Together with enantioselective indole dearomatization, these results demonstrate the power of the current biocatalytic platform in enabling enantioselective radical dearomatization of valuable heterocycles in an enzyme-controlled fashion. Additional examples of unsuccessful transformations are available in the Supplementary Information (Supplementary Fig. 8).

Enantioconvergent phenol dearomatase $P450_{rad4}$

Furthermore, we successfully extended this biocatalytic radical dearomatization platform to the conversion of other electron-rich aromatic substrates, such as phenols (Fig. 3). We were particularly interested in the radical dearomatization of racemic 2-bromo-1,3-dicarbonyl substrates (**5**), as these biocatalytic processes would give rise to spirocyclic products possessing contiguous quaternary–quaternary stereocentres in an enantioconvergent fashion. In this effort, $P450_{arc1}$ L266H G438T L78C ('P2'), an intermediate aromatic radical cyclase variant we previously engineered, was identified as a promising hit, providing dearomatized product in 28% yield and 71:29 e.r. (Supplementary Tables 3 and 19). With **5a** as the model substrate, by targeting active-site residues, four rounds of site-saturation mutagenesis and screening provided $P450_{rad4}$ bearing four beneficial mutations, including F437P, L436A, L75F and G268P (Fig. 3a). With this final variant $P450_{rad4}$, biocatalytic conversion of racemic **5a** led to enantio-enriched dearomatized product **6a** in 98% yield, 100% conversion and 94:6 e.r., furnishing a rare example of an enantioconvergent radical dearomatization protocol (Supplementary Table 19). The 6-*endo-trig* radical cyclization to phenol's *meta* position was not observed under these conditions.

With phenol dearomatase $P450_{rad4}$, this enantioconvergent radical dearomatization was found to be compatible with a range of phenolic substrates (Fig. 3b). Unsubstituted phenol (**5b**) and 2,6-disubstituted phenols (**5a** and **5c**) underwent enantioconvergent radical dearomatization with excellent yields and enantioselectivities. Ester groups with varying sizes, including ethyl (**6a**–**6c**), propyl (**6d**) and butyl (**6e**) esters, were all compatible with this radical biotransformation. Using the starting variant P2, highly sterically congested product **6f** bearing adjacent quaternary–quaternary carbons and 3,5-dimethyl substituents could be obtained in 45% yield and 78:22 e.r. Finally, when unsymmetric phenol **5g** was applied, the same P2 variant provided **6g** featuring a quaternary–quaternary stereochemical dyad in a diastereo- and enantioselective manner (55% yield, 81:19 d.r. and 84:16 e.r.). For biocatalytic reactions providing modest yields, the reduced and uncyclized compound was found to be the major side product. The relative stereochemistry of the major diastereomer of **6g** was determined by two-dimensional (2D) nuclear Overhauser effect spectroscopy (NOESY) analysis (Supplementary Section VI for details). Additionally, the absolute stereochemistry of dearomatized product **6a** was also determined by X-ray diffraction analysis (CCDC no. 2245161).

Nanomicelle-accelerated biocatalytic radical dearomatization

During our investigation on biocatalytic dearomatization of phenol derivatives, we discovered a notable micelle effect in accelerating the biotransformation of naphthol substrates with a very low solubility in water. In our early studies on the dearomatization of naphthol **7a**, we found that a previously engineered P450 variant P411-CIS T438S ($P450_{rad5}$; ref. 49) exhibited promising levels of enantiocontrol (89:11 e.r.), albeit with low yield (9%; Supplementary Table 4 for details). The exceedingly low levels of solubility and dispersivity of substrate **7a** in water led us to hypothesize that the low effective concentration of the substrate, and not the enzyme activity, represented the bottleneck for the further optimization of this biotransformation. Consistent with this hypothesis, subsequent studies revealed an important co-solvent effect, and higher yields and slightly better enantioselectivities were achieved by changing the co-solvent from ethanol (9% yield and 89:11 e.r.) to dimethyl sulfoxide (DMSO; 21% yield and 91:9 e.r.). Further increasing the volume percentage of the co-solvent from 4% to 40% did not result in further improvements (Supplementary Table 21). Thus, alternative strategies are required to further enhance the efficiency of these biotransformations.

We envisioned that micellar catalysis could afford a general solution to this solubility problem, as the hydrophobic core of nanomicelles composed of amphiphiles would provide an excellent environment to house hydrophobic substrates, thus significantly increasing their effective concentration. Meanwhile, the judicious selection of surfactants will allow for the maintenance of metalloenzyme integrity and catalytic activity. Previous studies revealed that in contrast to widely used ionic surfactants, non-ionic surfactants do not lead to protein denaturation and are therefore excellent candidates for the proposed nanomicelle-accelerated biocatalysis[50]. To this end, six designer non-ionic surfactants, including those recently developed by the Lipshutz group[51–53], were evaluated (Table 1). The inclusion of non-ionic surfactants (2 wt%) resulted in improved yield of **8a**, confirming the nanomicelle effect on this radical biotransformation. The use of Brij 30 and Brij 35 furnished 83% and 85% **8a**, respectively, although with reduced enantioselectivities (62:38 e.r. and 68:32 e.r.; Table 1, entries 2 and 3). The addition of 2 wt% MC-1 (ref. 51), a previously developed non-ionic surfactant with a sulfoxide functional group, provided a similar activity with a slightly reduced enantioselectivity (entry 4). Additionally, TPGS-750-M (ref. 52) and Nok (ref. 53) displayed similar effects in enhancing the efficiency of biocatalysis (57% and 58% yield, respectively; entries 5 and 6). Furthermore, tocopherol-derived designer surfactant TPGS-1000 was found to be the most efficient in facilitating this biocatalytic dearomatization, affording **8a** in 71% yield and 92:8 e.r. (entry 7). In general, the use of surfactants with a terminal hydroxy group (Brij 30, Brij 35 and TPGS-1000) allowed for higher conversions and yields to be achieved relative to those with a terminal methoxy group (Nok and TPGS-750-M). Moreover, this beneficial surfactant effect can be translated into biotransformations with cell-free lysates, providing further improved yields and enantioselectivities (84% yield and 97:3 e.r.; entry 8 and entry 9). Taken together, these results provided a rare demonstration of substantial micelle acceleration in both whole-cell biocatalysis and lysate biocatalysis, underscoring the importance of the judicious choice of surfactants to facilitate biotransformations. We expect this strategy to find applications in other new-to-nature biocatalytic processes involving substrates with a low aqueous solubility.

https://doi.org/10.1038/s41557-024-01608-8

Table 1 | Evaluation of P411-CIS T438S as the catalyst for enantioselective radical dearomatization of 7a with surfactants

Entry[a]	Surfactant	e.r.	Yield (%)	Total turnover number
1[b]	-	91:9	21±3	650±80
2	Brij 30	62:38	83±2	1,890±40
3	Brij 35	68:32	85±1	1,930±30
4	MC-1	84:16	21±1	470±20
5	Nok	91:9	57±4	1,300±90
6	TPGS-750-M	89:11	58±4	1,330±90
7	TPGS-1000	92:8	71±5	1,630±120
8[c]	**TPGS-1000**	**97:3**	**84±4**	**1,510±80**
9[d]	-	97:3	33±3	600±60

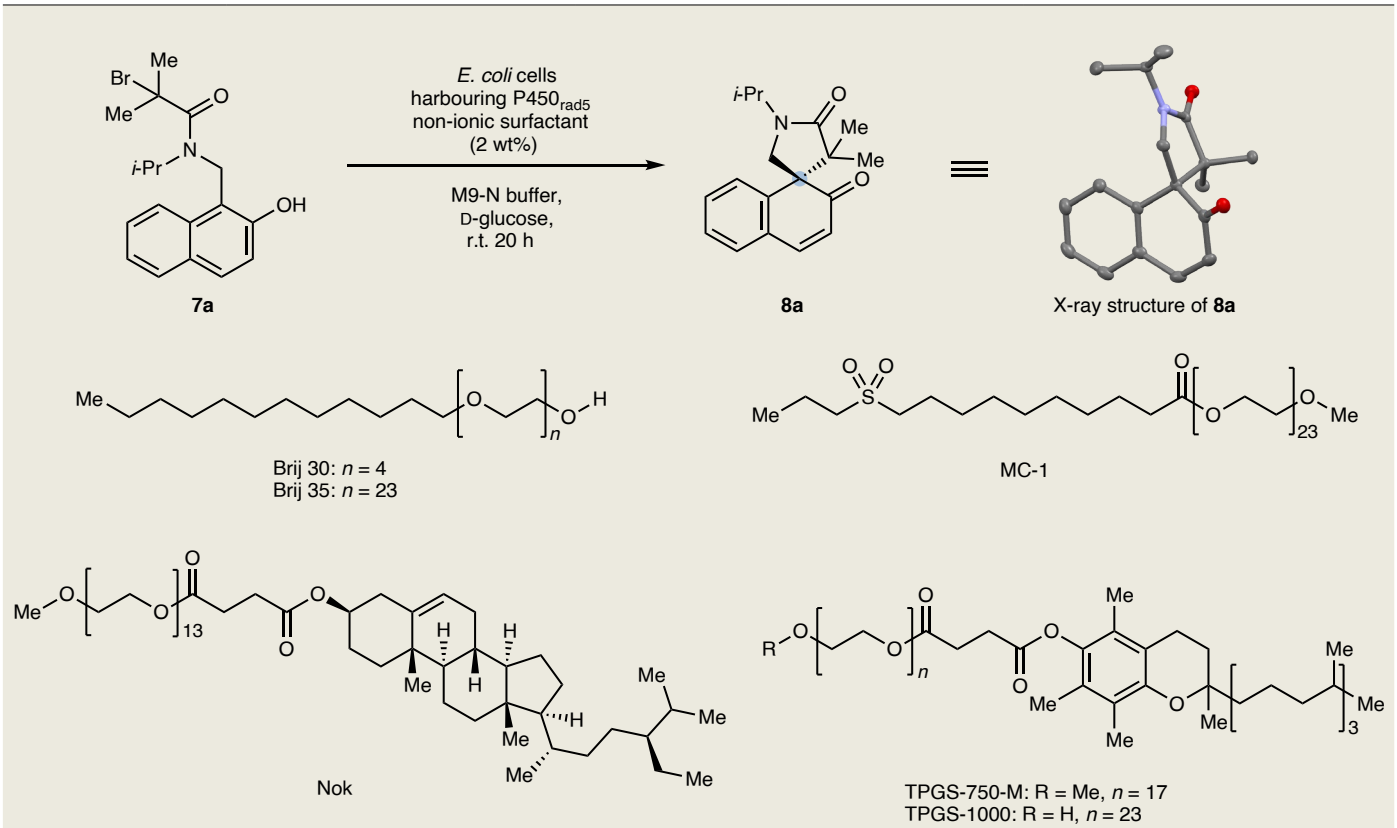

[a]All reactions using $P450_{rad5}$ were run in triplicate using whole *E. coli* cells (OD_{600}=30) with substrate **7a** (5 mM, 2 μmol), D-glucose (50 mM) and surfactant (2 wt%) in M9-N buffer (total volume, 400 μl). OD_{600} is the optical density of a cell sample measured at a wavelength of 600 nm in 1 cm light path. [b]Reactions using $P450_{rad5}$ were run in triplicate using whole *E. coli* cells (OD_{600}=30) without any surfactants. [c]Reactions using $P450_{rad5}$ were run in triplicate using cell-free lysate (OD_{600}=30) with **7a** (5.0 mM), sodium ascorbate (5.0 mM) and surfactant (2 wt%) in M9-N buffer (total volume, 400 μl). Bold indicates the best result from these optimizations. [d]Reactions using $P450_{rad5}$ were run in triplicate using cell-free lysate (OD_{600}=30) with **7a** (5.0 mM) and sodium ascorbate (5.0 mM) without any surfactant. For X-ray crystal structures, thermal ellipsoids were set at 50% probability; hydrogen atoms are omitted for clarity. All the biocatalytic reactions were performed as technical triplicates.

Computational insights into enzymatic enantiocontrol

To gain insights into the enantiocontrol in this biocatalytic radical dearomatization, we carried out molecular dynamics (MD) simulations to model the enzyme–substrate interactions of $P450_{rad1}$ with both enantiomers of the dearomatized intermediate **10a** formed after the radical addition and single electron transfer. As this cyclized product resembles the enantioselectivity-determining transition state[54], we reasoned that these MD simulations would reveal key active-site residues responsible for ensuring excellent enantioselectivity in radical dearomatization. Our MD simulations indicate that the two enantiomers **(*S*)-10a** and **(*R*)-10a** exhibit contrasting binding poses within the active site. While the *N*-*i*-Pr group of **(*S*)-10a** and **(*R*)-10a** prefers to point towards the hydrophobic pocket next to A82 and A264, the polar N–H moiety of the indole is placed at different orientations. In the enzyme complex with **(*S*)-10a**, which leads to the major enantiomeric product **(*S*)-2a**, the N–H bond forms a strong hydrogen bond with the hydroxyl group on T438, as evidenced by a short most-populated $N–H^{sub}\cdots O^{T438}$ distance of 3.3 Å (Fig. 4a shows the distributions of $H^{sub}\cdots O^{T438}$ distance along the MD trajectories; sub, substrate), as well as molecular mechanics with generalized Born and surface area solvation (MM-GBSA) substrate–residue interaction energy calculations (Supplementary Fig. 17). This hydrogen bonding interaction further anchors the reactive intermediate in the active site, resulting in enhanced enantiocontrol with radical dearomatase $P450_{rad1}$. In the enzyme–**(*R*)-10a** complex, such a hydrogen bond is absent because the N–H moiety points towards the non-polar residue L75. This reveals the inability of $P450_{rad1}$ to stabilize this particular enantiomeric intermediate via hydrogen bonding, which agrees

https://doi.org/10.1038/s41557-024-01608-8

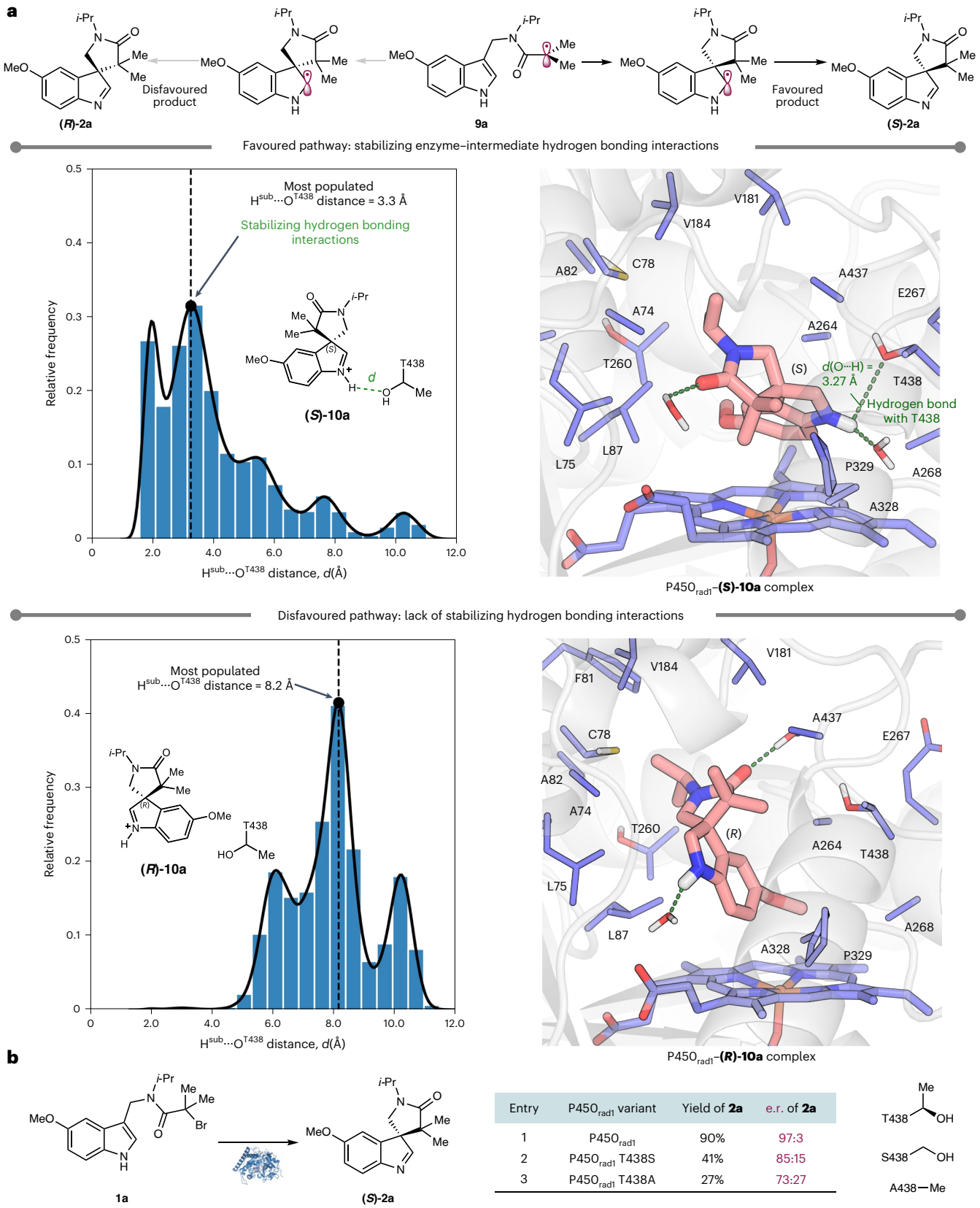

Entry	$P450_{rad1}$ variant	Yield of **2a**	e.r. of **2a**
1	$P450_{rad1}$	90%	97:3
2	$P450_{rad1}$ T438S	41%	85:15
3	$P450_{rad1}$ T438A	27%	73:27

Fig. 4 | Computational and experimental studies to shed light on the high levels of enantioselectivity observed with radical dearomatase $P450_{rad1}$. **a**, MD simulations with $P450_{rad1}$. Three replicas of independent 500 ns MD simulations were performed to model enzyme–substrate interactions with both enantiomers of the dearomatized intermediate **10a**. Top: Possible intermediates for the formation of both enantiomers of product **3a**. Left: Frequencies of the *d* value observed in MD simulations. Right: The most populated structure from MD simulations. The *d* value is the distance (H^{sub}···O^{T438} distance) as shown in the figure. **b**, Experimental studies to validate the key role of T438 of $P450_{rad1}$. All the biocatalytic reactions were performed as technical triplicates, with conditions as follows: **1a** (5.0 mM), sodium ascorbate (5.0 mM) and cell-free lysates with OD_{600} = 120 in M9-N buffer (total volume, 400 µl). Supplementary Table 23 contains details.

https://doi.org/10.1038/s41557-024-01608-8

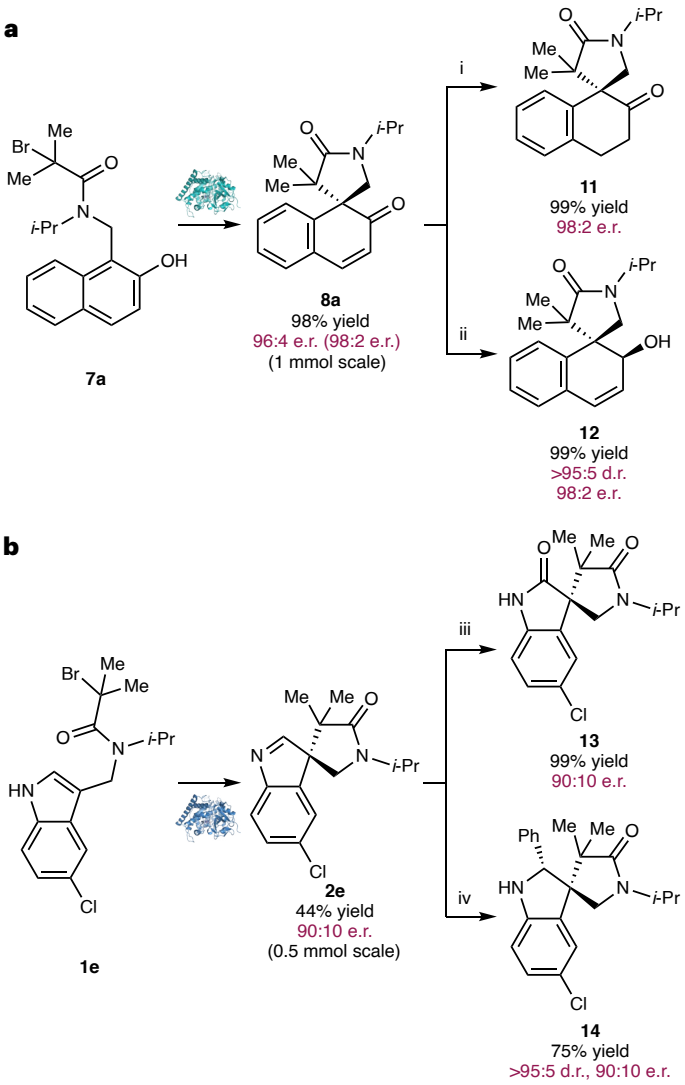

Fig. 5 | Preparative-scale biocatalytic radical dearomatization and derivatization of dearomatized products. a, Preparative-scale biocatalytic radical dearomatization of **7a** and transformation of dearomatized product **8a**. **b**, Preparative-scale biocatalytic radical dearomatization of **1e** and transformation of dearomatized product **2e**. Conditions were as follows: i, 10 wt% Pd/C, H_2 (1 atm), EtOAc, r.t. and 24 h; ii, $NaBH_4$ (1.2 equiv.), MeOH, r.t. and 6 h; iii, $NaClO_2$ (5.0 equiv.), NaH_2PO_4 (1.5 equiv.), 2-methyl-2-butene (10 equiv.), THF/H_2O, r.t. and 4 h; and iv, CuCl (2.5 mol%), PhMgBr (5.0 equiv.), toluene, reflux and 18 h. THF, tetrahydrofuran. In **a**, the 98:2 e.r. of **8a** was obtained after a single recrystallization.

with the experimentally observed enantioselectivity favouring the (*S*)-enantiomer of the cyclized product.

To experimentally validate the proposed role of T438, we generated $P450_{rad1}$ T438X mutants (X = serine (S) and alanine (A)) by site-directed mutagenesis and evaluated their activity and enantioselectivity (Fig. 4b). S438 with a hydroxyl group can potentially serve as a hydrogen bond donor akin to T438, while A438 lacks a hydrogen donor. When T438 was replaced by S438, lower levels of activity and enantioselectivity were observed (41% yield, 85:15 e.r.; Fig. 4b, entry 2). Furthermore, $P450_{rad1}$ T438A afforded further reduced activity and enantioselectivity (27% yield, 73:27 e.r.; entry 3). These experimental results supported the key role of the hydroxyl group of T438 in engaging the substrate through a hydrogen bonding interaction, leading to further enhanced enzymatic activity and enantiocontrol in the radical dearomatization of **1a**. Thus, together with our previous studies on our P450 atom transfer radical cyclase $P450_{ATRCase1}$ (ref. 21), the present computational study suggested bifunctional enzyme catalysis as a general mechanism to further enhance enzyme efficiency and stereocontrol in new-to-nature biocatalytic transformations.

Transformation of radical dearomatization products

To further demonstrate the synthetic utility of our newly developed biocatalytic asymmetric radical dearomatization, we performed these biotransformations on a 0.5–1.0 mmol scale and carried out downstream derivatization reactions (Fig. 5). Using cell-free lysates, in these preparative-scale biocatalytic processes, **(*R*)-8a** was isolated in 98% yield and 96:4 e.r., while **(*S*)-2e** was isolated in 44% yield and 90:10 e.r. Furthermore, starting from **(*R*)-8a**, C=C double bond hydrogenation with Pd/C afforded ketone **11** in 99% yield and 98:2 e.r. with excellent chemoselectivity[55]. Additionally, selective carbonyl reduction of this α,β-unsaturated ketone with $NaBH_4$ (ref. 56) generated stereochemically well-defined alcohol **12** in quantitative yield, >95:5 d.r. and 98:2 e.r. Starting from **(*S*)-2e**, Pinnick oxidation[57] afforded oxindole **(*S*)-13** in quantitative yield and 90:10 e.r. Finally, copper(I)-catalysed addition of phenylmagnesium to imine **2e** (ref. 58) proceeded in a highly diastereoselective manner, giving rise to **(2*S*,3*S*)-14** in 75% yield, >95:5 d.r. and 90:10 e.r. The relative stereochemistry of **14** was ascertained by 2D NOESY analysis (Supplementary Section VII for details).

Discussion

In this study, P450 radical dearomatases were evolved to allow the asymmetric radical dearomatization of indoles, pyrroles and phenols bearing a pendant α-halocarbonyl radical precursor. Together with our prior work on P450 atom transfer radical cyclases[20,21] and aromatic radical cyclases[23], these results showed that a unifying haem-enabled radical initiation and cyclization mechanism could allow for multiple synthetically valuable asymmetric transformations to be developed, thus demonstrating the synthetic utility of this evolvable biocatalyst platform.

In summary, we developed a biocatalytic strategy for asymmetric radical dearomatization using a new-to-nature metalloredox mechanism. Directed evolution of radical dearomatases allowed a wide range of aromatic and heteroaromatic compounds, including phenols, indoles and pyrroles, to be transformed with excellent stereocontrol, giving rise to dearomatized products featuring adjacent quaternary–quaternary stereocentres. Notably, the excellent tunability of these P450 radical dearomatases allowed both enantiodivergent and enantioconvergent radical transformations to be conveniently developed, further demonstrating the adaptable nature of this metalloenzyme platform. Combined computational and experimental studies unveiled the importance of additional hydrogen bonding interactions between the engineered enzyme and the reactive intermediate, indicating bifunctional biocatalysis as a useful strategy to enhance the activity and enantioselectivity of metalloenzyme catalysts. Furthermore, a surprising nanomicelle acceleration effect was discovered, providing an alternative tactic to facilitate otherwise sluggish new-to-nature biocatalytic processes. Overall, the ability to impose excellent stereocontrol over challenging free-radical-mediated transformations highlighted the potential of unnatural metalloredox biocatalysis to solve long-standing problems in asymmetric catalysis.

Online content

Any methods, additional references, Nature Portfolio reporting summaries, source data, extended data, supplementary information, acknowledgements, peer review information; details of author contributions and competing interests; and statements of data and code availability are available at https://doi.org/10.1038/s41557-024-01608-8.

References

1. von Ragué Schleyer, P. Introduction: aromaticity. *Chem. Rev.* **101**, 1115–1118 (2001).

2. Zheng, C. & You, S.-L. Catalytic asymmetric dearomatization (CADA) reaction-enabled total synthesis of indole-based natural products. *Nat. Prod. Rep.* **36**, 1589–1605 (2019).
3. Wertjes, W. C., Southgate, E. H. & Sarlah, D. Recent advances in chemical dearomatization of nonactivated arenes. *Chem. Soc. Rev.* **47**, 7996–8017 (2018).
4. Zhuo, C.-X., Zhang, W. & You, S.-L. Catalytic asymmetric dearomatization reactions. *Angew. Chem. Int. Ed.* **51**, 12662–12686 (2012).
5. Zheng, C. & You, S.-L. Advances in catalytic asymmetric dearomatization. *ACS Cent. Sci.* **7**, 432–444 (2021).
6. Roche, S. P. & Porco, J. A. Jr. Dearomatization strategies in the synthesis of complex natural products. *Angew. Chem. Int. Ed.* **50**, 4068–4093 (2011).
7. Wang, Y., Zhang, W.-Y., Yu, Z.-L., Zheng, C. & You, S.-L. SmI_2-mediated enantioselective reductive dearomatization of non-activated arenes. *Nat. Synth.* **1**, 401–406 (2022).
8. Zhang, W.-Y., Wang, H.-C., Wang, Y., Zheng, C. & You, S.-L. Enantioselective dearomatization of indoles via SmI_2-mediated intermolecular reductive coupling with ketones. *J. Am. Chem. Soc.* **145**, 10314–10321 (2023).
9. Proctor, R. S. J., Colgan, A. C. & Phipps, R. J. Exploiting attractive non-covalent interactions for the enantioselective catalysis of reactions involving radical intermediates. *Nat. Chem.* **12**, 990–1004 (2020).
10. Mondal, S. et al. Enantioselective radical reactions using chiral catalysts. *Chem. Rev.* **122**, 5842–5976 (2022).
11. Sibi, M. P., Manyem, S. & Zimmerman, J. Enantioselective radical processes. *Chem. Rev.* **103**, 3263–3296 (2003).
12. Bloom, J. D. & Arnold, F. H. In the light of directed evolution: pathways of adaptive protein evolution. *Proc. Natl Acad. Sci. USA* **106**, 9995–10000 (2009).
13. Reetz, M. T. Laboratory evolution of stereoselective enzymes: a prolific source of catalysts for asymmetric reactions. *Angew. Chem. Int. Ed.* **50**, 138–174 (2011).
14. Bornscheuer, U. T. et al. Engineering the third wave of biocatalysis. *Nature* **485**, 185–194 (2012).
15. Gibson, D. T., Koch, J. R. & Kallio, R. E. Oxidative degradation of aromatic hydrocarbons by microorganisms. I. Enzymic formation of catechol from benzene. *Biochemistry* **7**, 2653–2662 (1968).
16. Boyd, D. R. & Bugg, T. D. H. Arene *cis*-dihydrodiol formation: from biology to application. *Org. Biomol. Chem.* **4**, 181–192 (2006).
17. Johnson, R. A. Microbial arene oxidations. In *Organic Reactions* (ed. Overman, L. E.) 117–264 (John Wiley & Sons, 2004).
18. Baker Dockrey, S. A., Lukowski, A. L., Becker, M. R. & Narayan, A. R. H. Biocatalytic site- and enantioselective oxidative dearomatization of phenols. *Nat. Chem.* **10**, 119–125 (2018).
19. Jacoby, C. et al. Channeling C1 metabolism toward *S*-adenosylmethionine-dependent conversion of estrogens to androgens in estrogen-degrading bacteria. *mBio* **11**, https://doi.org/10.1128/mbio.01259-20 (2020).
20. Zhou, Q., Chin, M., Fu, Y., Liu, P. & Yang, Y. Stereodivergent atom-transfer radical cyclization by engineered cytochromes P450. *Science* **374**, 1612–1616 (2021).
21. Fu, Y. et al. Engineered P450 atom-transfer radical cyclases are bifunctional biocatalysts: reaction mechanism and origin of enantioselectivity. *J. Am. Chem. Soc.* **144**, 13344–13355 (2022).
22. Rui, J. et al. Directed evolution of nonheme iron enzymes to access abiological radical-relay C(sp^3)–H azidation. *Science* **376**, 869–874 (2022).
23. Fu, W. et al. Enzyme-controlled stereoselective radical cyclization to arenes enabled by metalloredox biocatalysis. *Nat. Catal.* **6**, 628–636 (2023).
24. Emmanuel, M. A. et al. Photobiocatalytic strategies for organic synthesis. *Chem. Rev.* **123**, 5459–5520 (2023).
25. Emmanuel, M. A., Greenberg, N. R., Oblinsky, D. G. & Hyster, T. K. Accessing non-natural reactivity by irradiating nicotinamide-dependent enzymes with light. *Nature* **540**, 414–417 (2016).
26. Biegasiewicz, K. F. et al. Photoexcitation of flavoenzymes enables a stereoselective radical cyclization. *Science* **364**, 1166–1169 (2019).
27. Black, M. J. et al. Asymmetric redox-neutral radical cyclization catalysed by flavin-dependent 'ene'-reductases. *Nat. Chem.* **12**, 71–75 (2020).
28. Clayman, P. D. & Hyster, T. K. Photoenzymatic generation of unstabilized alkyl radicals: an asymmetric reductive cyclization. *J. Am. Chem. Soc.* **142**, 15673–15677 (2020).
29. Page, C. G. et al. Quaternary charge-transfer complex enables photoenzymatic intermolecular hydroalkylation of olefins. *J. Am. Chem. Soc.* **143**, 97–102 (2021).
30. Gao, X., Turek-Herman, J. R., Choi, Y. J., Cohen, R. D. & Hyster, T. K. Photoenzymatic synthesis of α-tertiary amines by engineered flavin-dependent "ene"-reductases. *J. Am. Chem. Soc.* **143**, 19643–19647 (2021).
31. Nicholls, B. T. et al. Engineering a non-natural photoenzyme for improved photon efficiency. *Angew. Chem. Int. Ed.* **61**, e202113842 (2022).
32. Fu, H. et al. An asymmetric sp^3–sp^3 cross-electrophile coupling using 'ene'-reductases. *Nature* **610**, 302–307 (2022).
33. Fu, H., Qiao, T., Carceller, J. M., MacMillan, S. N. & Hyster, T. K. Asymmetric *C*-alkylation of nitroalkanes *via* enzymatic photoredox catalysis. *J. Am. Chem. Soc.* **145**, 787–793 (2023).
34. Page, C. G. et al. Regioselective radical alkylation of arenes using evolved photoenzymes. *J. Am. Chem. Soc.* **145**, 11866–11874 (2023).
35. Harrison, W., Huang, X. & Zhao, H. Photobiocatalysis for abiological transformations. *Acc. Chem. Res.* **55**, 1087–1096 (2022).
36. Huang, X. et al. Photoenzymatic enantioselective intermolecular radical hydroalkylation. *Nature* **584**, 69–74 (2020).
37. Huang, X. et al. Photoinduced chemomimetic biocatalysis for enantioselective intermolecular radical conjugate addition. *Nat. Catal.* **5**, 586–593 (2022).
38. Cheng, L. et al. Stereoselective amino acid synthesis by synergistic photoredox-pyridoxal radical biocatalysis. *Science* **381**, 444–451 (2023).
39. Quasdorf, K. W. & Overman, L. E. Catalytic enantioselective synthesis of quaternary carbon stereocentres. *Nature* **516**, 181–191 (2014).
40. Süsse, L. & Stoltz, B. M. Enantioselective formation of quaternary centers by allylic alkylation with first-row transition-metal catalysts. *Chem. Rev.* **121**, 4084–4099 (2021).
41. Poulos, T. L. Heme enzyme structure and function. *Chem. Rev.* **114**, 3919–3962 (2014).
42. Phillips, I. R., Shephard, E. A. & Ortiz de Montellano, P. R. *Cytochrome P450 Protocols* (Humana, 2013).
43. Brandenberg, O. F., Fasan, R. & Arnold, F. H. Exploiting and engineering hemoproteins for abiological carbene and nitrene transfer reactions. *Curr. Opin. Biotechnol.* **47**, 102–111 (2017).
44. Yang, Y. & Arnold, F. H. Navigating the unnatural reaction space: directed evolution of heme proteins for selective carbene and nitrene transfer. *Acc. Chem. Res.* **54**, 1209–1225 (2021).
45. Mukaiyama, T., Ogata, K., Sato, I. & Hayashi, Y. Asymmetric organocatalyzed Michael addition of nitromethane to a 2-oxoindoline-3-ylidene acetaldehyde and the three one-pot sequential synthesis of (−)-horsfiline and (−)-coerulescine. *Chem. Eur. J.* **20**, 13583–13588 (2014).
46. Díaz-Marrero, A. R. et al. Carijodienone from the octocoral *Carijoa multiflora*. A spiropregnane-based steroid. *J. Nat. Prod.* **74**, 292–295 (2011).

47. Bandini, M. & Eichholzer, A. Catalytic functionalization of indoles in a new dimension. *Angew. Chem. Int. Ed.* **48**, 9608–9644 (2009).
48. Brandenberg, O. F. et al. Stereoselective enzymatic synthesis of heteroatom-substituted cyclopropanes. *ACS Catal.* **8**, 2629–2634 (2018).
49. McIntosh, J. A. et al. Enantioselective intramolecular C—H amination catalyzed by engineered cytochrome P450 enzymes in vitro and in vivo. *Angew. Chem. Int. Ed.* **52**, 9309–9312 (2013).
50. Højgaard, C., Sørensen, H. V., Pedersen, J. S., Winther, J. R. & Otzen, D. E. Can a charged surfactant unfold an uncharged protein? *Biophys. J.* **115**, 2081–2086 (2018).
51. Cortes-Clerget, M. et al. MC-1. A "designer" surfactant engineered for peptide synthesis in water at room temperature. *Green Chem.* **21**, 2610–2614 (2019).
52. Lipshutz, B. H. et al. TPGS-750-M: a second-generation amphiphile for metal-catalyzed cross-couplings in water at room temperature. *J. Org. Chem.* **76**, 4379–4391 (2011).
53. Klumphu, P. & Lipshutz, B. H. "Nok": a phytosterol-based amphiphile enabling transition-metal-catalyzed couplings in water at room temperature. *J. Org. Chem.* **79**, 888–900 (2014).
54. Noey, E. L. et al. Origins of stereoselectivity in evolved ketoreductases. *Proc. Natl Acad. Sci. USA* **112**, E7065–E7072 (2015).
55. Xu, R.-Q., Yang, P., Tu, H.-F., Wang, S.-G. & You, S.-L. Palladium(0)-catalyzed intermolecular arylative dearomatization of β-naphthols. *Angew. Chem. Int. Ed.* **55**, 15137–15141 (2016).
56. Hu, J. et al. Pd-catalyzed dearomative asymmetric allylic alkylation of naphthols with alkoxyallenes. *J. Org. Chem.* **85**, 7896–7904 (2020).
57. Mohamed, M. A., Yamada, K. & Tomioka, K. Accessing the amide functionality by the mild and low-cost oxidation of imine. *Tetrahedron Lett.* **50**, 3436–3438 (2009).
58. Wang, G., Lu, R., He, C. & Liu, L. Kinetic resolution of indolines by asymmetric hydroxylamine formation. *Nat. Commun.* **12**, 2512 (2021).

Methods

Expression of P450$_{rad}$ variants

Escherichia coli (*E. cloni* BL21(DE3)) cells carrying P450$_{rad}$-encoding plasmid were grown overnight in 3 ml of Luria-Bertani medium with 0.1 mg ml^{-1} ampicillin (LB$_{amp}$). Preculture (1.5 ml) was used to inoculate 28.5 ml of Hyperbroth (AthenaES) with 0.1 mg ml^{-1} ampicillin (HB$_{amp}$) in a 125 ml Erlenmeyer flask. This culture was incubated at 37 °C and 230 rpm for 2 h. It was then cooled on ice for 20 min and induced with 0.5 mM isopropyl β-D-1-thiogalactopyranoside (IPTG) and 1.0 mM 5-aminolevulinic acid (final concentrations). Expression was conducted at 22 °C and 150 rpm for 20 h. *E. coli* cells were then transferred to a 50 ml conical tube and pelleted by centrifugation (3,000*g*, 5 min, 4 °C). Supernatant was removed and the resulting cell pellet was resuspended in M9-N buffer to OD$_{600}$ = 5–240 (usually 30–60). An aliquot of this cell suspension (2 ml) was taken to determine protein concentration using the haemochrome assay after lysis by sonication.

Asymmetric radical dearomatization using cell-free lysate of P450$_{rad}$

Suspensions of *E. coli* (*E. cloni* BL21(DE3)) cells expressing the appropriate P450$_{rad}$ variant in M9-N buffer (2 ml, typically OD$_{600}$ = 30–240) were lysed by sonication using an ultrasonic homogenizer equipped with a stepped microtip (6 min in total, 1 s on, 1 s off, 40% amplitude, two cycles); samples were submerged in wet ice during sonication. The resulting lysate was centrifuged (21,130*g*, 4 °C, 10 min) to remove the cell debris. The supernatant was separated from the pellet and kept on ice until use.

To a 2 ml sample vial was added the cell-free lysate containing P450$_{rad}$ (typically OD$_{600}$ = 30–240, 345 µl). This 2 ml vial was then transferred into an anaerobic chamber, where the organic substrate (15 µl of 133 mM stock solution in EtOH or DMSO) and sodium ascorbate (40 µl of 50 mM stock solution in M9-N buffer) were added. Final reaction volume was 400 µl; final concentrations were 5.0 mM substrate and 5.0 mM sodium ascorbate. Then vials were sealed and shaken on a microplate shaker at room temperature and 680 rpm for 12–24 h.

After 12–24 h, a solution of 1 mM 1,3,5-trimethoxybenzene or mesitylene (internal standard) in EtOAc (600 µl) was added. The mixture was transferred to a 1.5 ml centrifuge tube, vortexed (20 s each of three times) and centrifuged (21,130*g*, 5 min) to separate the organic and aqueous layers. The organic layers (350 µl per well) were transferred to 500 µl vial inserts, which were then placed in 2 ml vials and analysed by normal phase HPLC. CHIRALPAK IC/IB N-5/IG/IH columns were used for normal phase HPLC analysis.

Reporting summary

Further information on research design is available in the Nature Portfolio Reporting Summary linked to this article.

Data availability

All data are available in the main text and the Supplementary Information. Crystallographic data for compounds **2e**, **4a**, **6a** and **8a** reported in this Article have been deposited at the CCDC under deposition numbers 2245164 (**2e**), 2245162 (**4a**), 2245161 (**6a**) and 2245163 (**8a**). Copies of the data can be obtained free of charge via https://www.ccdc.cam.ac.uk/structures/. The raw data for the docking structures used in the Supplementary Information are also available from the authors upon reasonable request. Plasmids encoding evolved radical dearomatases reported in this study are available for research purposes from Y.Y. under a material transfer agreement with the University of California, Santa Barbara.

Acknowledgements

This research is supported by the National Institutes of Health (NIH; R35GM147387 to Y.Y. and R35GM128779 to P.L.). We acknowledge the National Science Foundation (NSF) BioPolymers, Automated Cellular Infrastructure, Flow, and Integrated Chemistry Materials Innovation Platform (BioPACIFIC MIP; DMR-1933487) and the NSF Materials Research Science and Engineering Center (MRSEC) at the University of California, Santa Barbara (DMR-2308708) for access to instrumentation. MD simulations were performed at the Center for Research Computing of the University of Pittsburgh and the Advanced Cyberinfrastructure Coordination Ecosystem: Services & Support (ACCESS) programme supported by the NSF, grant numbers OAC-2117681 and OAC-2138259. Y.F. is an Andrew W. Mellon Predoctoral Fellow. We thank Y.-M. Wang (University of Pittsburgh) for critical reading of this manuscript and B. Lipshutz (University of California, Santa Barbara) for the generous donation of surfactants used in this study.

Author contributions

Y.Y. conceived and directed the project. W.F., Y.Z. and H.W. prepared the substrates. W.F. and Y.Z. performed enzyme screening, enzyme engineering and substrate scope studies. Y.F. carried out the computational studies with P.L. providing guidance. Y.Y., P.L., W.F. and Y.F. wrote the manuscript with the input of all other authors.

Competing interests

Y.Y., W.F. and Y.Z. are inventors on a patent application (International Patent Application Serial No. PCT/US2023/085941) submitted by the University of California, Santa Barbara that covers compositions, methods and applications of evolved radical dearomatases. The remaining authors declare no competing interests.

Additional information

Supplementary information The online version contains supplementary material available at https://doi.org/10.1038/s41557-024-01608-8.

Correspondence and requests for materials should be addressed to Peng Liu or Yang Yang.

Peer review information *Nature Chemistry* thanks Zhongyue Yang and the other, anonymous, reviewer(s) for their contribution to the peer review of this work.

nature portfolio

Corresponding author(s): Yang Yang

Last updated by author(s): 05/26/2024

Reporting Summary

Nature Portfolio wishes to improve the reproducibility of the work that we publish. This form provides structure for consistency and transparency in reporting. For further information on Nature Portfolio policies, see our Editorial Policies and the Editorial Policy Checklist.

Statistics

For all statistical analyses, confirm that the following items are present in the figure legend, table legend, main text, or Methods section.

n/a	Confirmed	
☐	☒	The exact sample size (*n*) for each experimental group/condition, given as a discrete number and unit of measurement
☒	☐	A statement on whether measurements were taken from distinct samples or whether the same sample was measured repeatedly
☒	☐	The statistical test(s) used AND whether they are one- or two-sided *Only common tests should be described solely by name; describe more complex techniques in the Methods section.*
☒	☐	A description of all covariates tested
☒	☐	A description of any assumptions or corrections, such as tests of normality and adjustment for multiple comparisons
☐	☒	A full description of the statistical parameters including central tendency (e.g. means) or other basic estimates (e.g. regression coefficient) AND variation (e.g. standard deviation) or associated estimates of uncertainty (e.g. confidence intervals)
☒	☐	For null hypothesis testing, the test statistic (e.g. *F*, *t*, *r*) with confidence intervals, effect sizes, degrees of freedom and *P* value noted *Give P values as exact values whenever suitable.*
☒	☐	For Bayesian analysis, information on the choice of priors and Markov chain Monte Carlo settings
☒	☐	For hierarchical and complex designs, identification of the appropriate level for tests and full reporting of outcomes
☒	☐	Estimates of effect sizes (e.g. Cohen's *d*, Pearson's *r*), indicating how they were calculated

Our web collection on statistics for biologists contains articles on many of the points above.

Software and code

Policy information about availability of computer code

Data collection	Autogrid4 and Autodock4 were used for primary docking
Data analysis	mgltools_win32_1.5.7 was used for the analysis of docking results

For manuscripts utilizing custom algorithms or software that are central to the research but not yet described in published literature, software must be made available to editors and reviewers. We strongly encourage code deposition in a community repository (e.g. GitHub). See the Nature Portfolio guidelines for submitting code & software for further information.

Data

Policy information about availability of data

All manuscripts must include a data availability statement. This statement should provide the following information, where applicable:

- Accession codes, unique identifiers, or web links for publicly available datasets
- A description of any restrictions on data availability
- For clinical datasets or third party data, please ensure that the statement adheres to our policy

All data are available in the main text and the Supplementary Information. Crystallographic data for compounds 2e, 4a, 6a and 8a reported in this Article has been deposited at the Cambridge Crystallographic Data Centre under deposition number CCDC 2245164, 2245162, 2245161 and 2245163. Copies of the data can be obtained free of charge via https://www.ccdc.cam.ac.uk/structures/. The raw data for the docking structures used in the Supporting Information is also available

from the authors upon reasonable request. Plasmids encoding evolved radical dearomatases reported in this study are available for research purposes from Y.Y. under a material transfer agreement with the University of California Santa Barbara.

Human research participants

Policy information about studies involving human research participants and Sex and Gender in Research.

Reporting on sex and gender	N/A
Population characteristics	N/A
Recruitment	N/A
Ethics oversight	N/A

Note that full information on the approval of the study protocol must also be provided in the manuscript.

Field-specific reporting

Please select the one below that is the best fit for your research. If you are not sure, read the appropriate sections before making your selection.

☒ Life sciences ☐ Behavioural & social sciences ☐ Ecological, evolutionary & environmental sciences

For a reference copy of the document with all sections, see nature.com/documents/nr-reporting-summary-flat.pdf

Life sciences study design

All studies must disclose on these points even when the disclosure is negative.

Sample size	All the biocatalytic reactions were performed in technical triplicates. Biological triplicates for substrates 1a, 3a, 5a, and 7a were performed. Triplicates are efficient enough to obtain yields and enantioselectivities of the biocatalytic reactions.
Data exclusions	No data was excluded.
Replication	All the biocatalytic reactions were performed in technical triplicates. Biological triplicates for substrates 1a, 3a, 5a, and 7a were performed. And all replications were successful and data was included.
Randomization	Randomization is not relevant to the study as the results of biocatalytic reactions are not dependent to randomization.
Blinding	Blinding is not relevant to the study as the output parameters are not subjective and therefore not subject to this form of bias.

Reporting for specific materials, systems and methods

We require information from authors about some types of materials, experimental systems and methods used in many studies. Here, indicate whether each material, system or method listed is relevant to your study. If you are not sure if a list item applies to your research, read the appropriate section before selecting a response.

Materials & experimental systems

n/a	Involved in the study
☒	☐ Antibodies
☒	☐ Eukaryotic cell lines
☒	☐ Palaeontology and archaeology
☒	☐ Animals and other organisms
☒	☐ Clinical data
☒	☐ Dual use research of concern

Methods

n/a	Involved in the study
☒	☐ ChIP-seq
☒	☐ Flow cytometry
☒	☐ MRI-based neuroimaging